Single-Dipole and Dual-Dipole Inverse Solutions in Electrocardiography

Vojko Jazbinšek and Rok Hren

Institute of Mathematics, Physics and Mechanics

vojko.jazbinsek@imfm.si

Mipro 2014, May 29

Introduction

- Mathematical modeling of both source and volume conductor remains one of the prerequisites for any quantitative interpretation of electrocardiographic data.
- One of the most often used approaches to solving the inverse problem in electrocardiography involves calculating the position and moment of an equivalent single dipole source in the model of the human torso
- The single dipole equivalent generator is adequate approximation only when the bioelectric activity of the heart is confined to a single very small volume, for example arising from ectopic foci and accessory pahtways between the atria and ventricles.
- In cases where more than one preexcitation is present, more complex equivalent generators (like two or more dipoles) would achieve better accuracy
- In this simulation study, we explored the possibility that approximation by two dipoles could be used to localize regional activation of dual accessory pathways.

Overview

I. Conducting sphere model

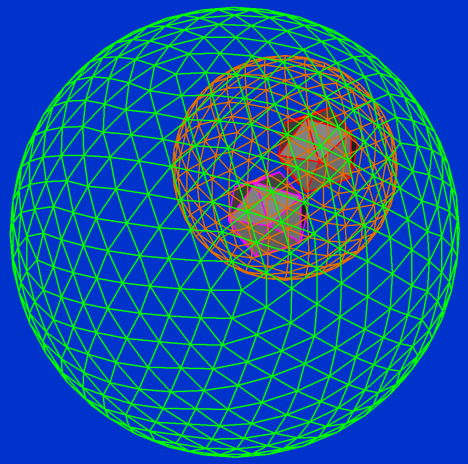

In the first part, we employed simple analytical conducting sphere model to evaluate single and dual dipole inverse solution for different:

- lead systems
- noise levels
- dual dipole source orientation
- dual dipole source distance

II. Anatomical computer model

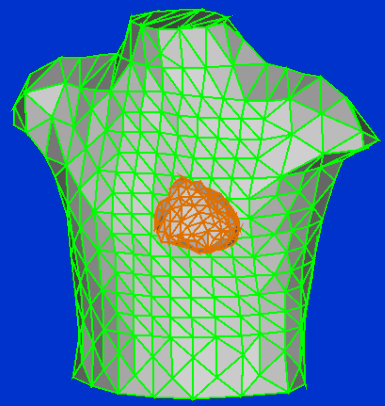

In the second part, we employed an anatomical computer model to asses the localization accuracy of two dipole inverse solution:

- single preexcitation sites
- dual preexcitation sites
- measurement noise level
- time after the onset of preexcitation
- presence of modeling errors

I. Conducting sphere model: Simulation protocol

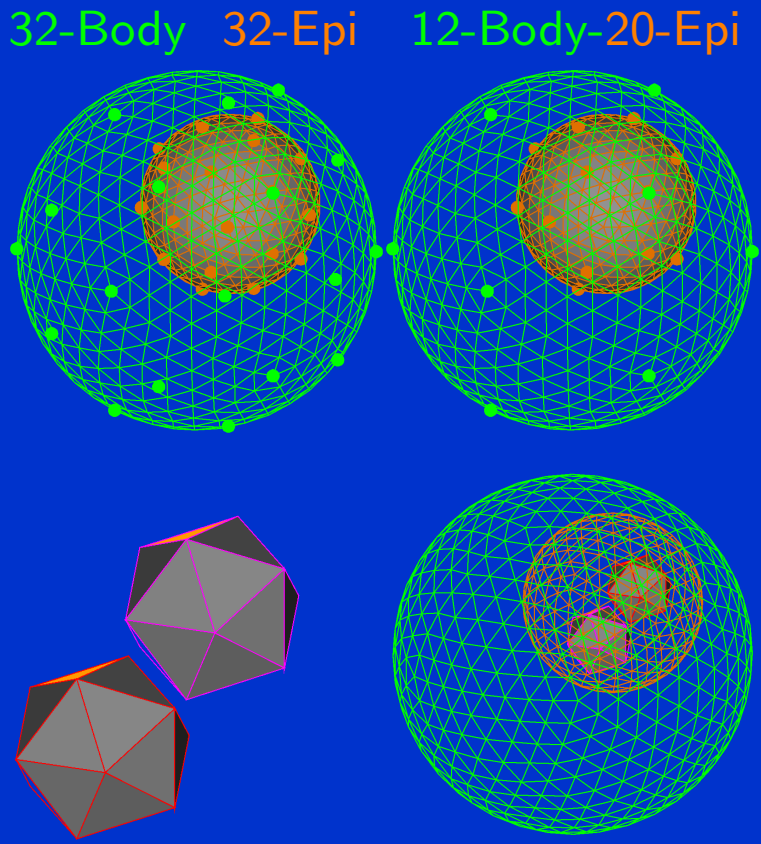

- outer (Body) sphere (R=1)
- inner (Epi) sphere (R=0.5), $\vec{r}_{\mathrm{E}} = (0.1, -0.2, 0.3)$
- three 32-leads systems
- single dipoles in 24 locations (nodes of two icosahedrons) in three directions
- for dual dipole sources, we combined
  - 12 most close (0.178 ± 0.069),
  - 12 most distant (0.696 ± 0.026),
  - 12 pairs of icosahedron nodes median distance ($||\vec{r}_{\mathrm{E}}|| = 0.374$)
  - In each of the pairs, we put either 3 parallel or anti-parallel or perpendicular dipoles pointing along axes of the coordinate system.
- for each calculated map we added 7 noise levels (10, 15,. . . 40 dB) and
- for each noise level, we generated 10 different noise distributions.

I. Results: Single dipoles in the conducting sphere model

Noise	32-Body			32-Epi			12-Body-20-Epi		
[dB]	$\Delta r/R \pm$SD	$RE_{fn} \pm$SD	$RE_{fa} \pm$SD	$\Delta r/R \pm$SD	$RE_{fn} \pm$SD	$RE_{fa} \pm$SD	$\Delta r/R \pm$SD	$RE_{fn} \pm$SD	$RE_{fa} \pm$SD
10	0.075±0.037	0.283±0.058	0.142±0.048	0.041±0.024	0.300±0.072	0.150±0.059	0.061±0.036	0.291±0.075	0.177±0.073
20	0.023±0.011	0.094±0.019	0.045±0.014	0.012±0.006	0.101±0.026	0.047±0.019	0.018±0.009	0.099±0.027	0.053±0.021
30	0.007±0.004	0.030±0.006	0.014±0.005	0.004±0.002	0.032±0.008	0.015±0.006	0.006±0.003	0.031±0.008	0.018±0.007
40	0.002±0.001	0.009±0.002	0.004±0.002	0.001±0.001	0.010±0.003	0.005±0.002	0.002±0.001	0.010±0.003	0.006±0.002

* Averaged over 720 samples (72 single dipole sources × 10 random noise distributions) for different lead systems and noise levels.

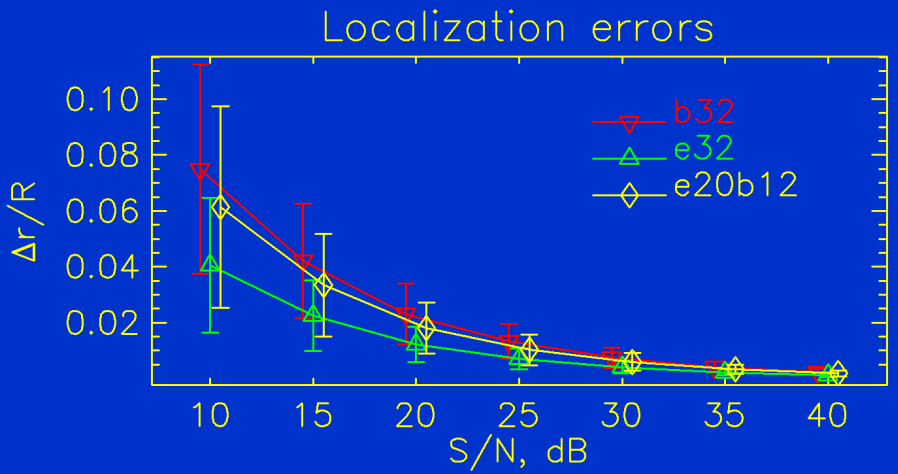

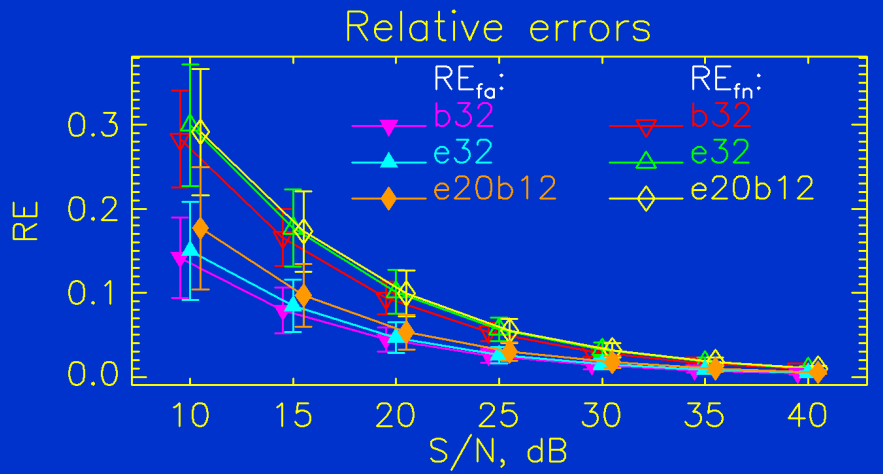

Localization errors:
$\Delta r = ||\vec{r}_f - \vec{r}_p||_2$, where

$||\mathbf{F}||_2 = \sqrt{\sum_i F_i^2}$ (2-norm).

Relative errors:

$$\mathrm{RE_{fn}} = \frac{||\mathbf{V_f} - \mathbf{V_n}||_2}{||\mathbf{V_n}||_2},$$

$$\mathrm{RE_{fa}} = \frac{||\mathbf{V_f} - \mathbf{V_a}||_2}{||\mathbf{V_a}||_2}.$$

I. Results: Single dipoles in the conducting sphere model

Noise	32-Body			32-Epi			12-Body-20-Epi		
[dB]	$\Delta r/R \pm$SD	$RE_{fn} \pm$SD	$RE_{fa} \pm$SD	$\Delta r/R \pm$SD	$RE_{fn} \pm$SD	$RE_{fa} \pm$SD	$\Delta r/R \pm$SD	$RE_{fn} \pm$SD	$RE_{fa} \pm$SD
10	0.075±0.037	0.283±0.058	0.142±0.048	0.041±0.024	0.300±0.072	0.150±0.059	0.061±0.036	0.291±0.075	0.177±0.073
20	0.023±0.011	0.094±0.019	0.045±0.014	0.012±0.006	0.101±0.026	0.047±0.019	0.018±0.009	0.099±0.027	0.053±0.021
30	0.007±0.004	0.030±0.006	0.014±0.005	0.004±0.002	0.032±0.008	0.015±0.006	0.006±0.003	0.031±0.008	0.018±0.007
40	0.002±0.001	0.009±0.002	0.004±0.002	0.001±0.001	0.010±0.003	0.005±0.002	0.002±0.001	0.010±0.003	0.006±0.002

* Averaged over 720 samples (72 single dipole sources × 10 random noise distributions) for different lead systems and noise levels.

Linear scale

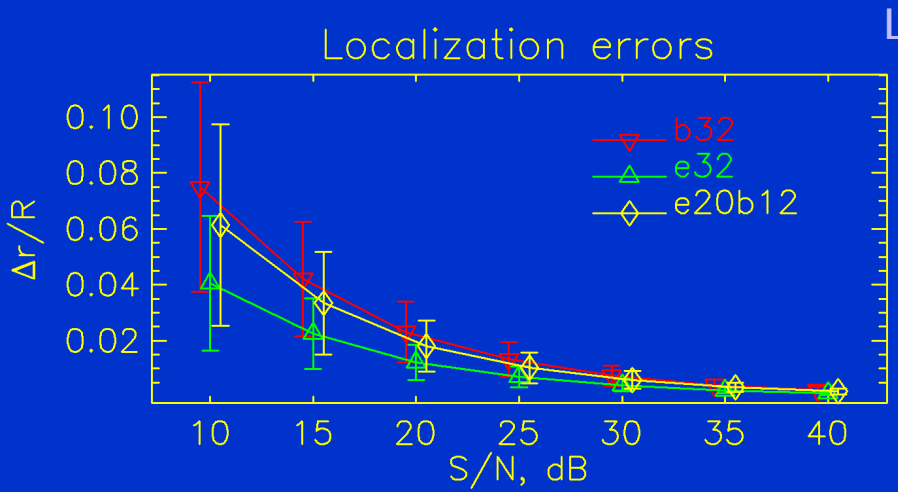

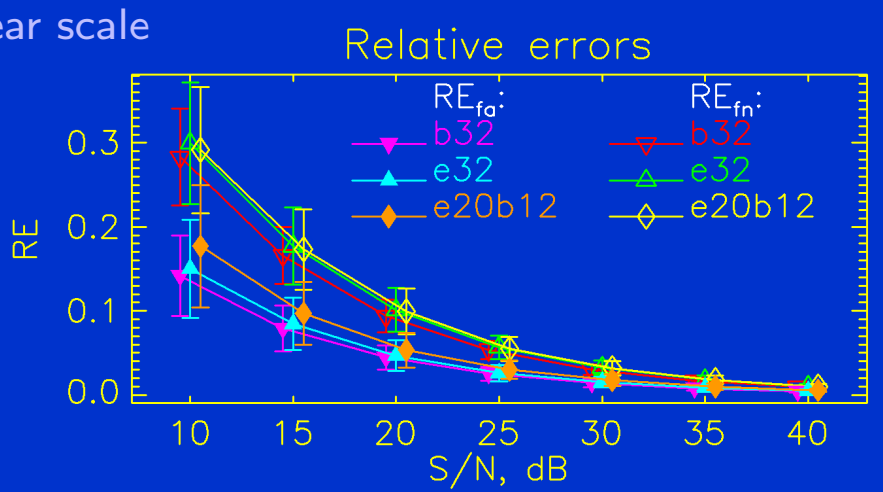

Localization errors:
$\Delta r = ||\vec{r}_f - \vec{r}_p||_2$, where

$||\mathbf{F}||_2 = \sqrt{\sum_i F_i^2}$ (2-norm).

Relative errors:

$$RE_{fn} = \frac{||\mathbf{V}_f - \mathbf{V}_n||_2}{||\mathbf{V}_n||_2},$$

$$RE_{fa} = \frac{||\mathbf{V}_f - \mathbf{V}_a||_2}{||\mathbf{V}_a||_2}.$$

Logarithmic scale

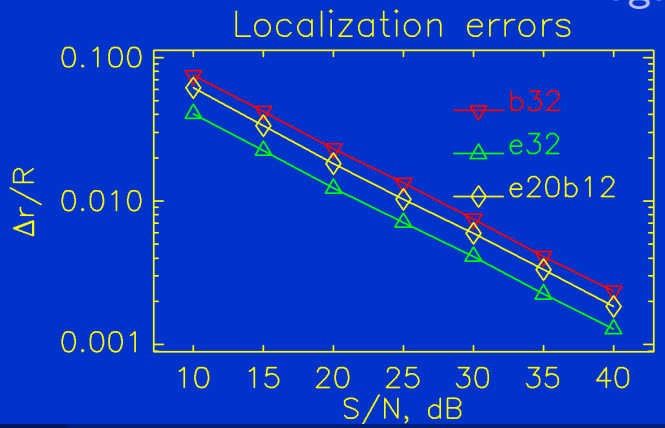

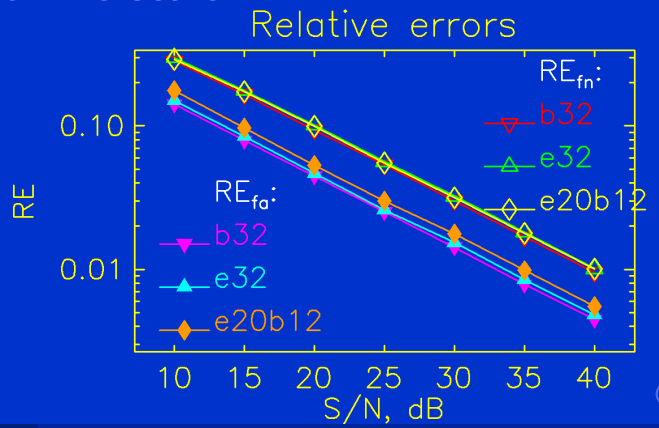

I. Results: Dual dipoles in the conducting sphere model

	S/N	Parallel dipoles					Anti-parallel dipoles					Perpendicular dipoles				
	[dB]	$\Delta r_1/R$	$\Delta r_2/R$	$\Delta r_c/R \pm$SD	RE_{fn}	RE_{fa}	$\Delta r_1/R$	$\Delta r_2/R$	$\Delta r_c/R \pm$SD	RE_{fn}	RE_{fa}	$\Delta r_1/R$	$\Delta r_2/R$	$\Delta r_c/R \pm$SD	RE_{fn}	RE_{fa}
close	10	0.163	0.162	0.262±0.123	0.223	0.206	0.197	0.204	0.291±0.163	0.590	1.389	0.160	0.161	0.247±0.115	0.300	0.293
	20	0.093	0.088	0.148±0.116	0.077	0.063	0.081	0.080	0.117±0.114	0.346	0.409	0.063	0.060	0.096±0.083	0.108	0.086
	30	0.033	0.031	0.051±0.077	0.025	0.020	0.029	0.029	0.042±0.047	0.149	0.128	0.022	0.021	0.033±0.034	0.034	0.027
	40	0.013	0.013	0.021±0.058	0.008	0.006	0.009	0.008	0.012±0.013	0.050	0.038	0.007	0.007	0.010±0.010	0.011	0.008
median	10	0.116	0.101	0.166±0.086	0.199	0.177	0.122	0.086	0.156±0.074	0.363	0.345	0.117	0.086	0.152±0.068	0.249	0.229
	20	0.033	0.031	0.048±0.026	0.068	0.054	0.030	0.030	0.045±0.022	0.134	0.106	0.030	0.026	0.042±0.018	0.088	0.067
	30	0.010	0.013	0.018±0.019	0.022	0.017	0.010	0.010	0.015±0.009	0.043	0.032	0.009	0.008	0.013±0.009	0.028	0.021
	40	0.003	0.003	0.005±0.003	0.007	0.005	0.003	0.003	0.005±0.004	0.013	0.011	0.003	0.003	0.004±0.002	0.008	0.007
distant	10	0.061	0.068	0.097±0.044	0.183	0.148	0.051	0.059	0.083±0.037	0.224	0.183	0.055	0.059	0.086±0.039	0.199	0.160
	20	0.018	0.021	0.029±0.018	0.059	0.047	0.017	0.021	0.029±0.019	0.075	0.057	0.018	0.021	0.030±0.018	0.065	0.051
	30	0.006	0.006	0.009±0.005	0.019	0.015	0.005	0.006	0.009±0.005	0.024	0.018	0.005	0.006	0.008±0.004	0.021	0.016
	40	0.002	0.002	0.003±0.001	0.006	0.005	0.002	0.002	0.003±0.001	0.007	0.006	0.002	0.002	0.003±0.001	0.007	0.005

** Averaged over 360 samples (36 dual dipole sources × 10 random noise distributions) for different S/N and groups of distances and orientations between two single dipoles that forming dual dipole sources. Combined error is defined as $\Delta r_c = \sqrt{\Delta r_1^2 + \Delta r_2^2}$.

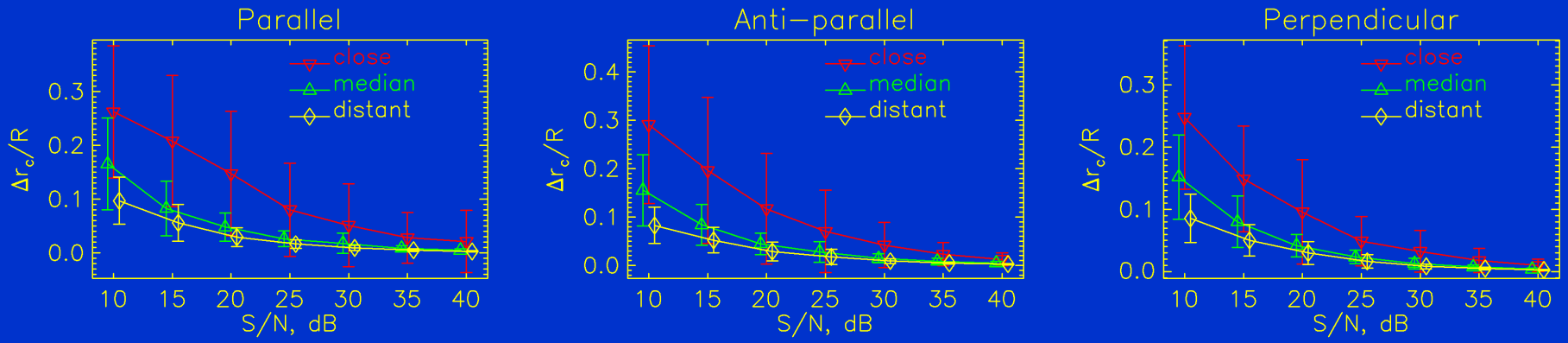

- Average localization errors depends on the distance between dipoles in the source model. In the presence of noise, locations of close positioned dipoles are poorly recovered
- Orientation between dipoles is not important.

II. Model of the human ventricular myocardium

Developed in Department of Physiology and Biophysics at Dalhousie University, Canada. Main features:

- an anatomically accurate geometry, with resolution of 0.5 mm (almost 1 800 000 elements)
- an intramural structure with rotating anisotropy
- propagation algorithm based on physiological principle of excitatory current flow (combination of cellular automaton and bidomain theory)

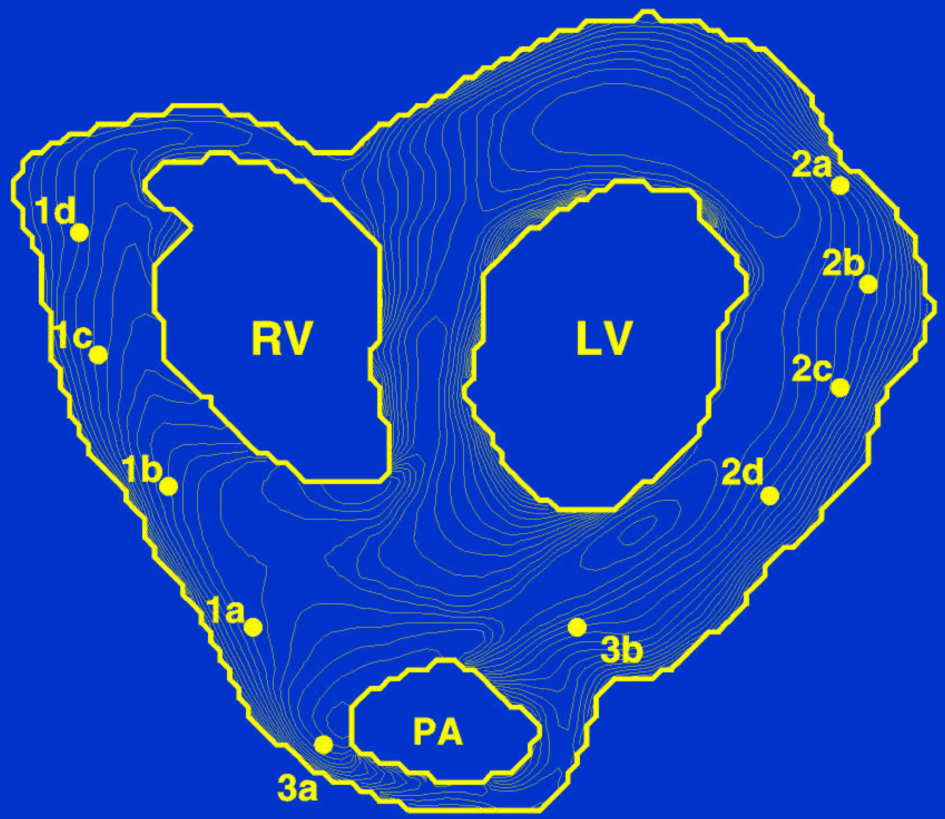

II. Preexcitation sites along the atrioventricular (AV) ring

10 single preexicitation sites:

Right sites:

posterolateral (RPL)

lateral (RL)

antrolateral (RAL)

anteroparaseptal (RAP)

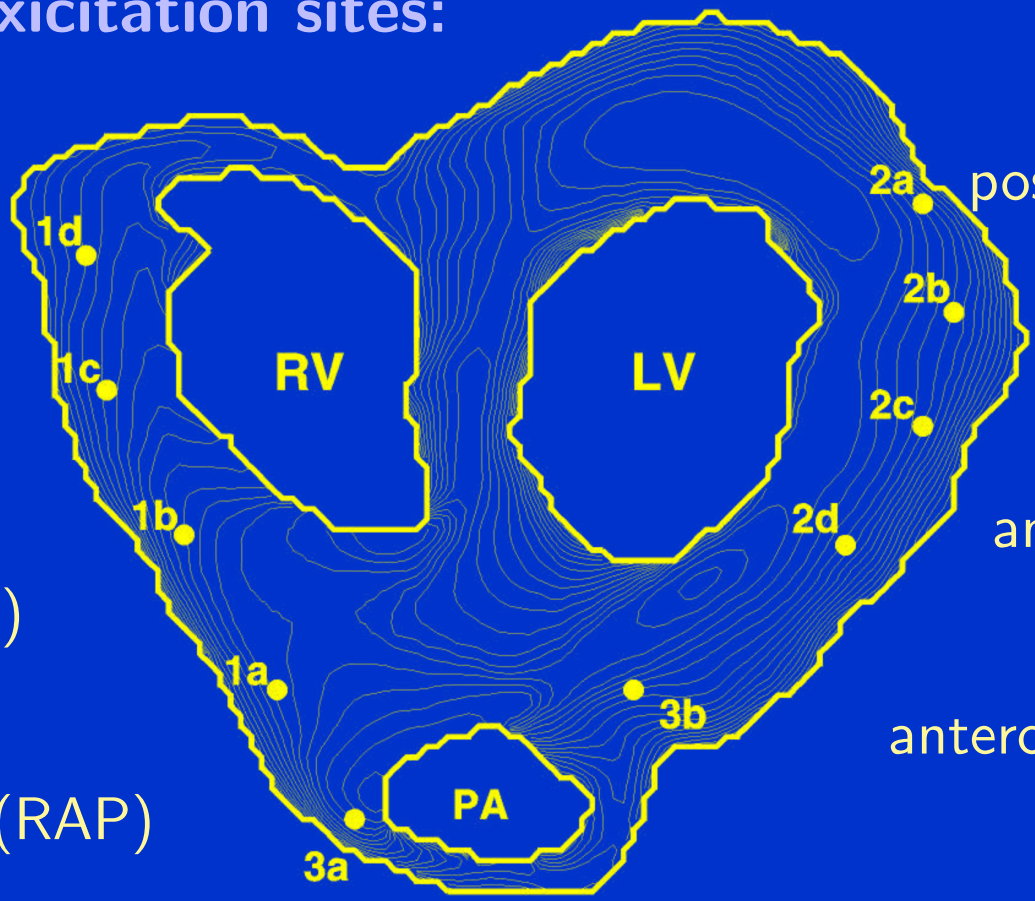

Left sites:

posterolateral (LPL)

lateral (LL)

anterolateral (LAL)

anteroparaseptal (LAP)

8 dual preexicitation sites:

1a-1b	RAL	(18)*	2a-2b	LPL/LL	(11)*	3a-3b	RAL/LAP	(30)*
1a-1c	RAL/RL	(34)	2a-2c	LPL/LL	(23)	1b-2b	RAL/RPL	(139)
1a-1d	RAL/RPL	(48)	2a-2d	LPL/LAL	(36)			

*Distance in mm between preexitation sites measured along AV ring

II. Anatomical ventricular model: Simulation protocol

- position an anatomical model of the human myocardium in the homogeneus torso model (Horacek) at hearts anatomical location
- simulate activation sequence with the ventricular model
- from this activation sequence, extracardiac electric potentials were calculated with the oblique dipole model of cardiac sources in combination with the boundary element torso model
- for each activation sequence we calculated 117-leads body surface potential map, covering anterior and posterior torso

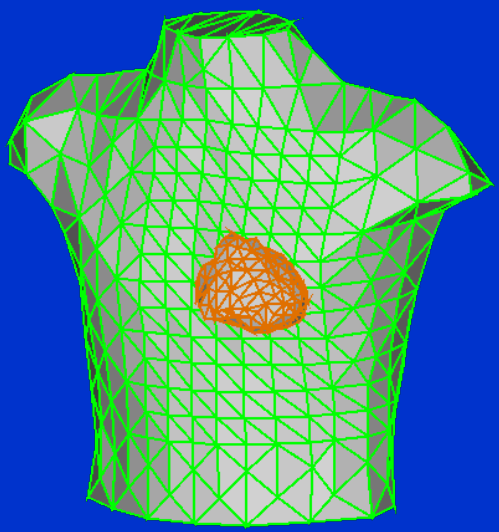

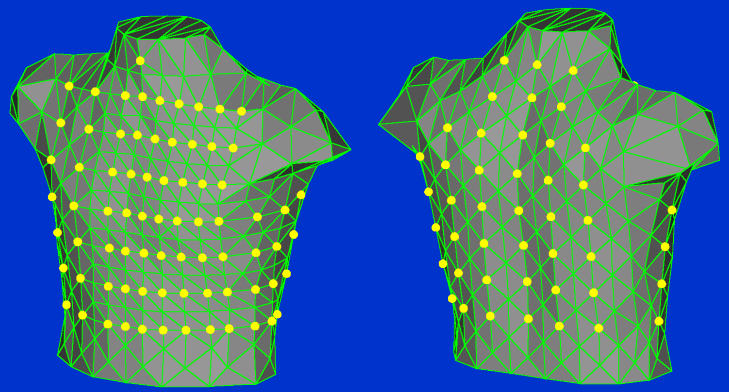

Anterior Posterior

- for each calculated map we added 4 noise levels (2.5, 5, 10, 20 μV)
- for each noise level, we generated 10 different noise distributions

II. Inverse solution protocol

Using simulated potential maps as input data, we performed the inverse solution for a pair of dipole sources in the torso model.

- initial estimates – dipole moments from several randomly selected starting dipole positions along the AV ring
- final localization with a Levenberg Marquardt least-square fitting procedure in the standard male torso
- localization error: distances between the best fitting pair of dipoles and a pair of preexcitation sites in the heart model
- rejected solutions: if the magnitude of a stronger of the two dipoles exceeds the weaker dipole by the factor of 5
- visual inspection: positions of reconstructed dipoles were superimposed on a realistic 3D epicardial surface

II. An example of the ventricular model validation study

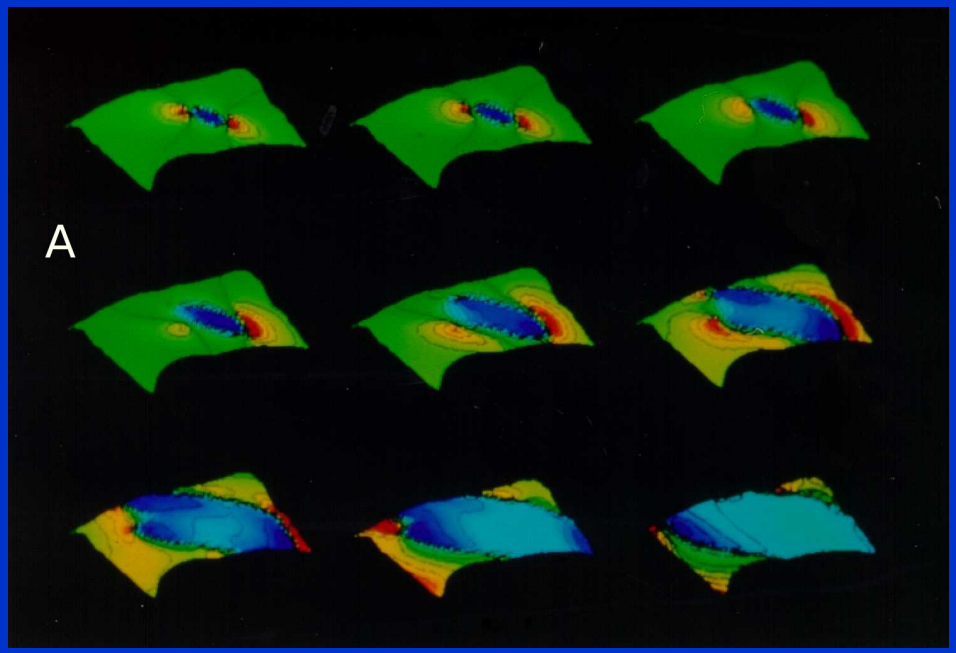

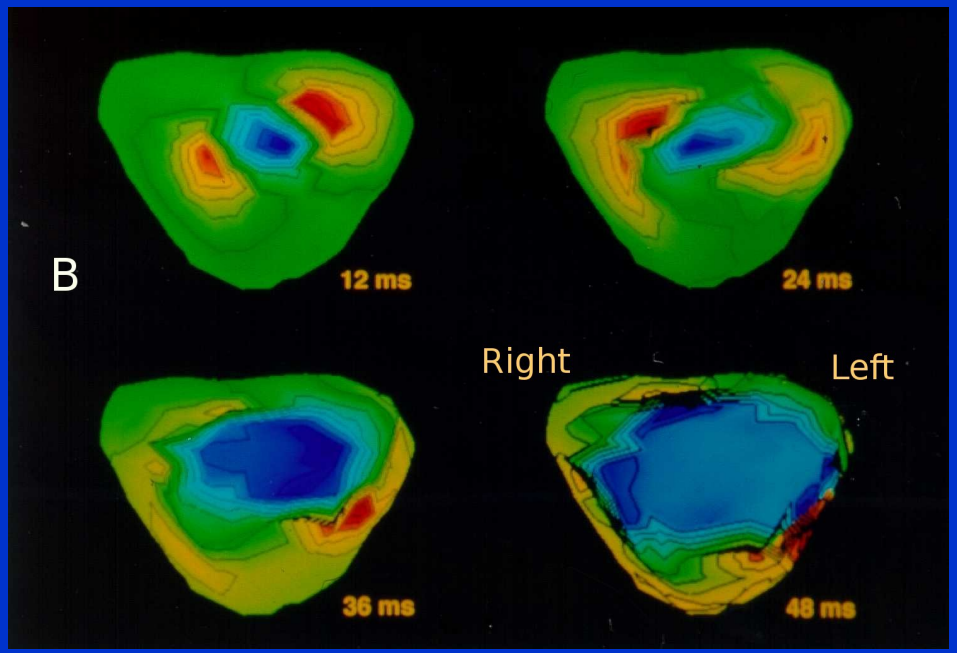

A – activation sequence is inserted into the endocardial site of the left apex
(4 ms steps are displayed)

B – epicardial surface potential maps, viewed from the anterior side.
– 12 ms after the activation onset there is one negative area and there are two adjacent positive areas, which later rotate CW.
– This is in agreement with fibers rotational anisotropy, which rotates CCW as we move from the endocardium to the epicardium.
– After the epicardium breaktrough (at 24 ms for this case), we observe large negative area.

II. An example of the ventricular model validation study

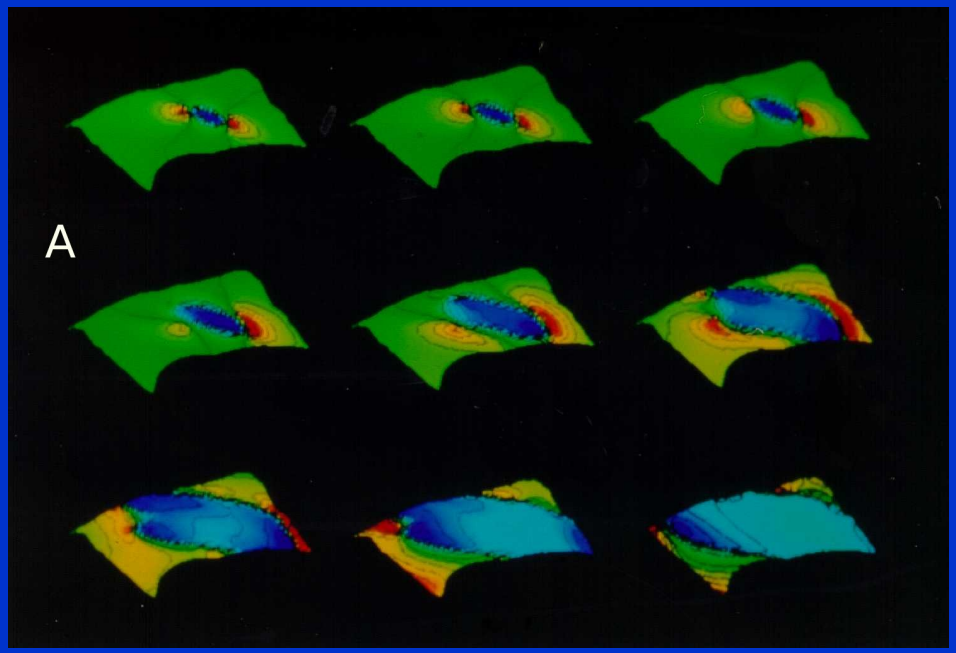

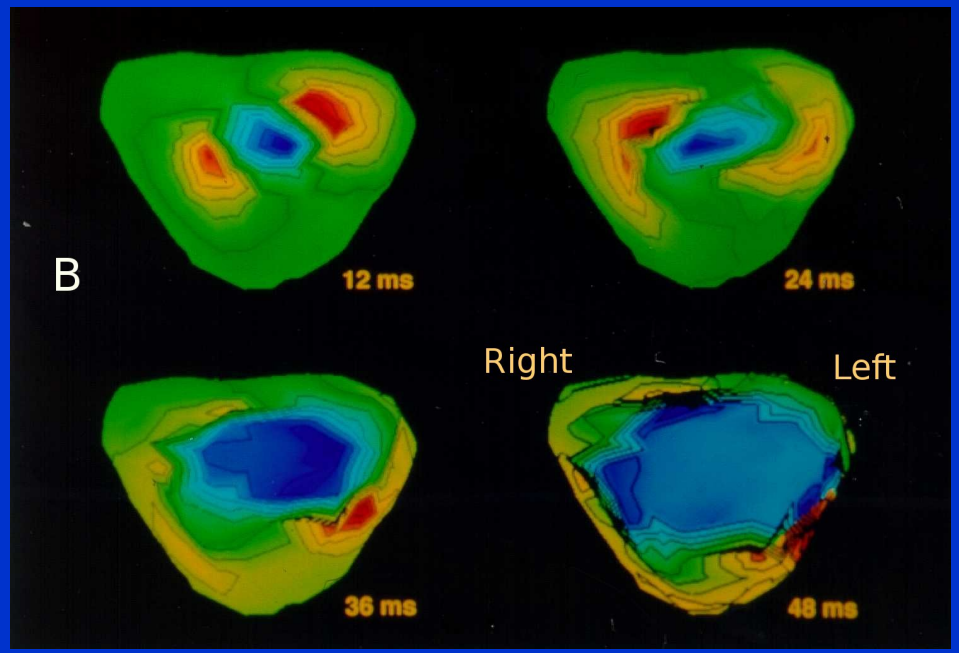

A – activation sequence is inserted into the endocardial site of the left apex (4 ms steps are displayed)

B – epicardial surface potential maps, viewed from the anterior side

C – corresponding BSPM sequence: Initially unstable pattern, characterized by low potential amplitudes ($< 100\ \mu$V), evolves into a distinct dipolar pattern.

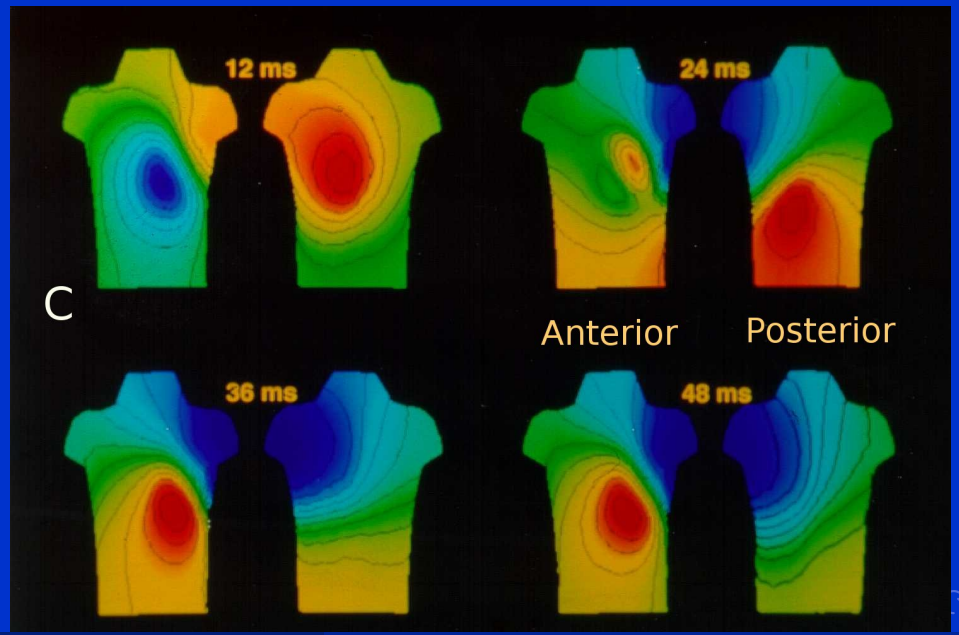

II. Early phases of excitation sequence – dual dipole source

- In the early phases of the activation sequence, one can clearly observe the formation of an elongated negative area above the pacing site and formation of two adjacent positive areas.

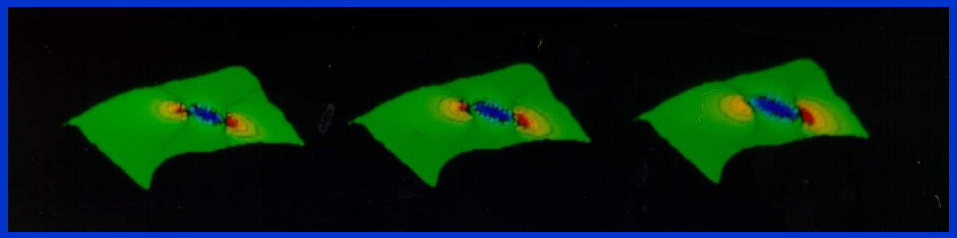

- This is in agreement with Macchi et al. [Acta Cardiol 47 (1992), 421-433] and Taccardi et al. [Circulation 90 (1994), 3076-3090] who pointed out that electric potentials during the initial phase of activation resemble those of two opposing dipoles oriented along the major axis and located near the ends of an elliptical wavefront of propagated activation.
- To test this hypothesis, we first assessed the performance of a two-dipole model in localizing single accessory pathways.

II. Left Lateral single accessory pathway

- projection of activation isochrone surface on the epicardial surface at different time instants (4 to 28 ms after the onset x)

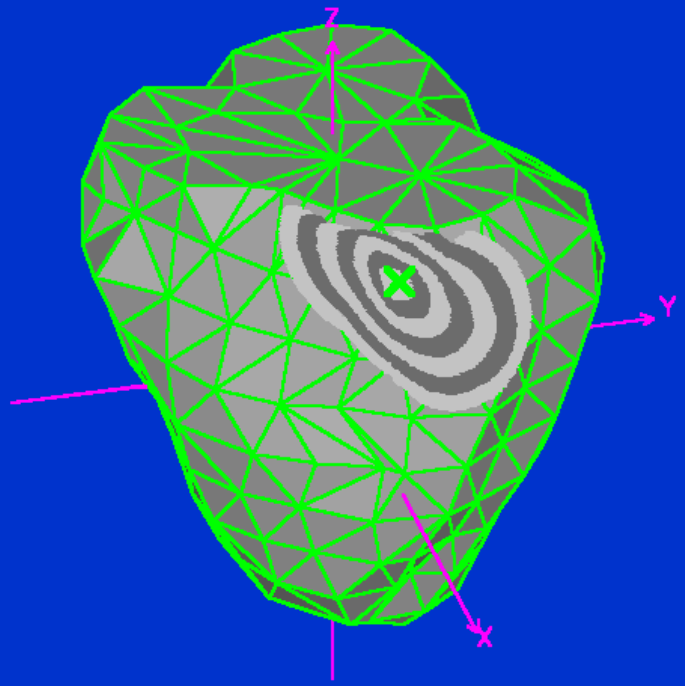

II. Left Lateral single accessory pathway

- projection of activation isochrone surface on the epicardial surface at different time instants (4 to 28 ms after the onset x)
- localization results obtained with a two dipole model (cyan and yellow)

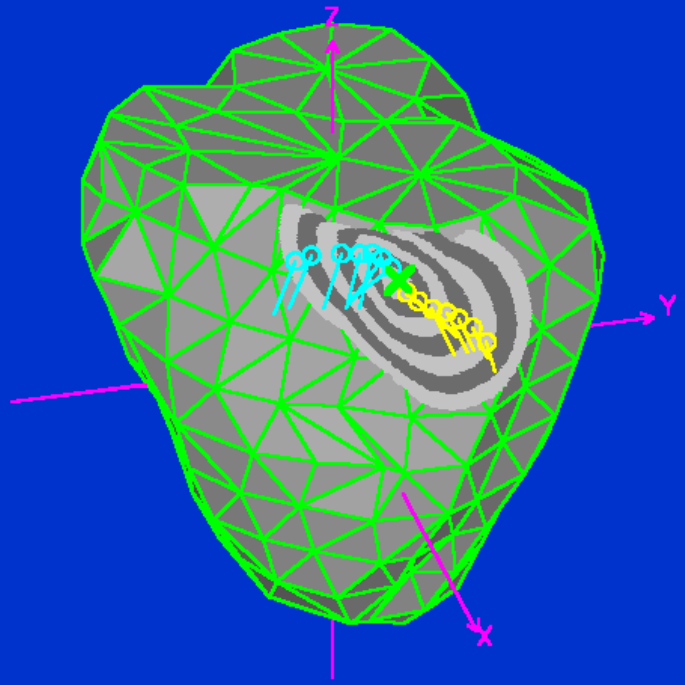

II. Left Lateral single accessory pathway

- projection of activation isochrone surface on the epicardial surface at different time instants (4 to 28 ms after the onset x)
- localization results obtained with a two dipole model (cyan and yellow)
- localization results obtained with a single dipole model (red)

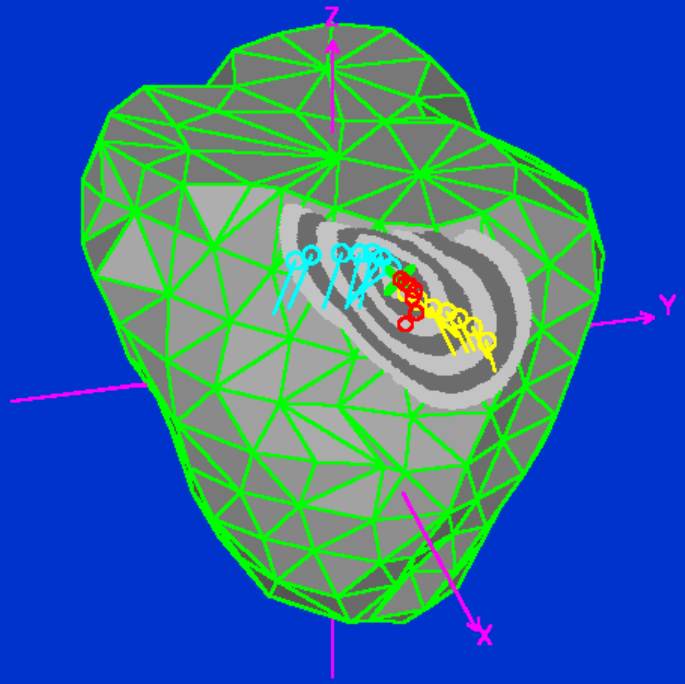

II. Left Lateral single accessory pathway

- projection of activation isochrone surface on the epicardial surface at different time instants (4 to 28 ms after the onset x)
- localization results obtained with a two dipole model (cyan and yellow)
- localization results obtained with a single dipole model (red)

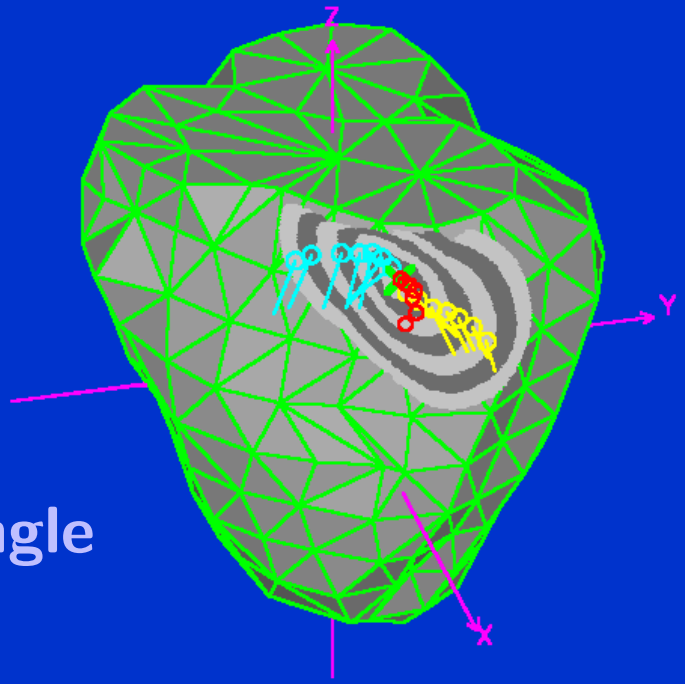

Average localization errors for all 10 single preexicitation sites in presence of noise

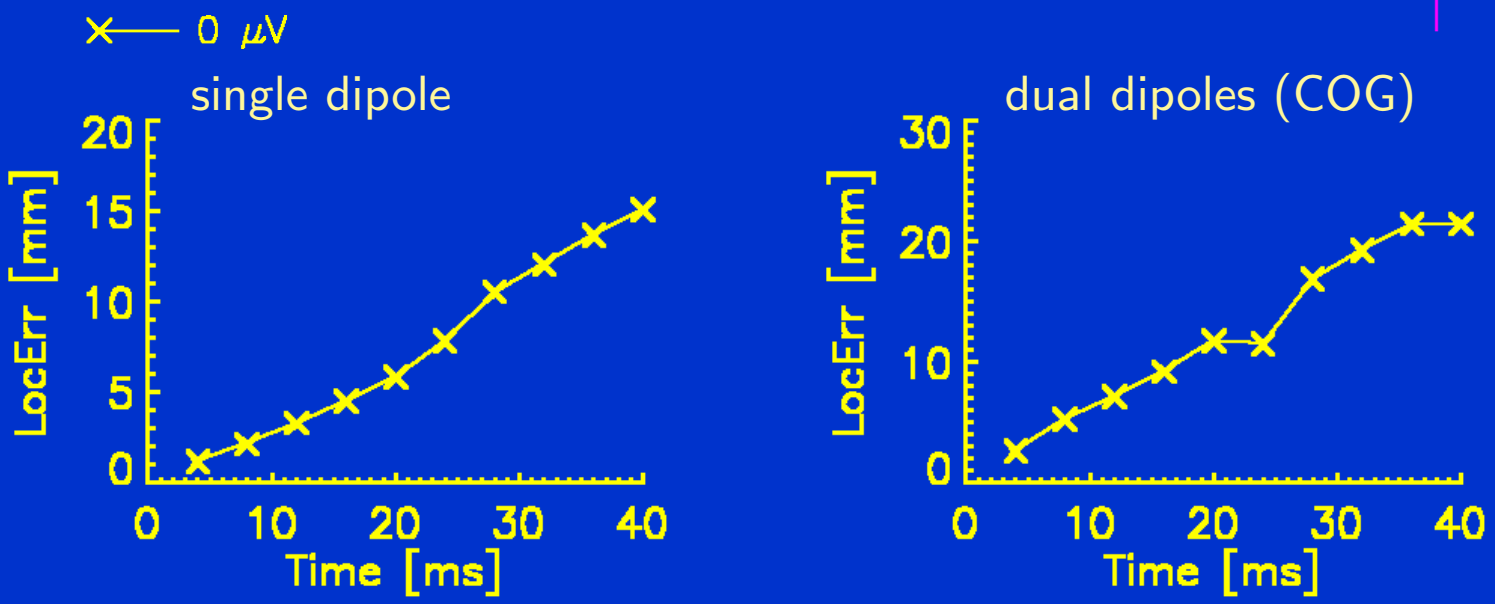

II. Left Lateral single accessory pathway

- projection of activation isochrone surface on the epicardial surface at different time instants (4 to 28 ms after the onset x)
- localization results obtained with a two dipole model (cyan and yellow)
- localization results obtained with a single dipole model (red)

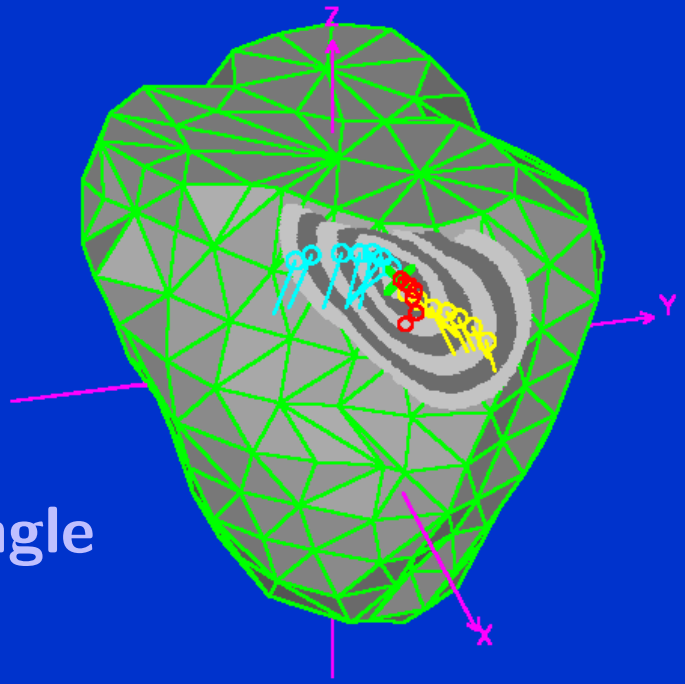

Average localization errors for all 10 single preexicitation sites in presence of noise

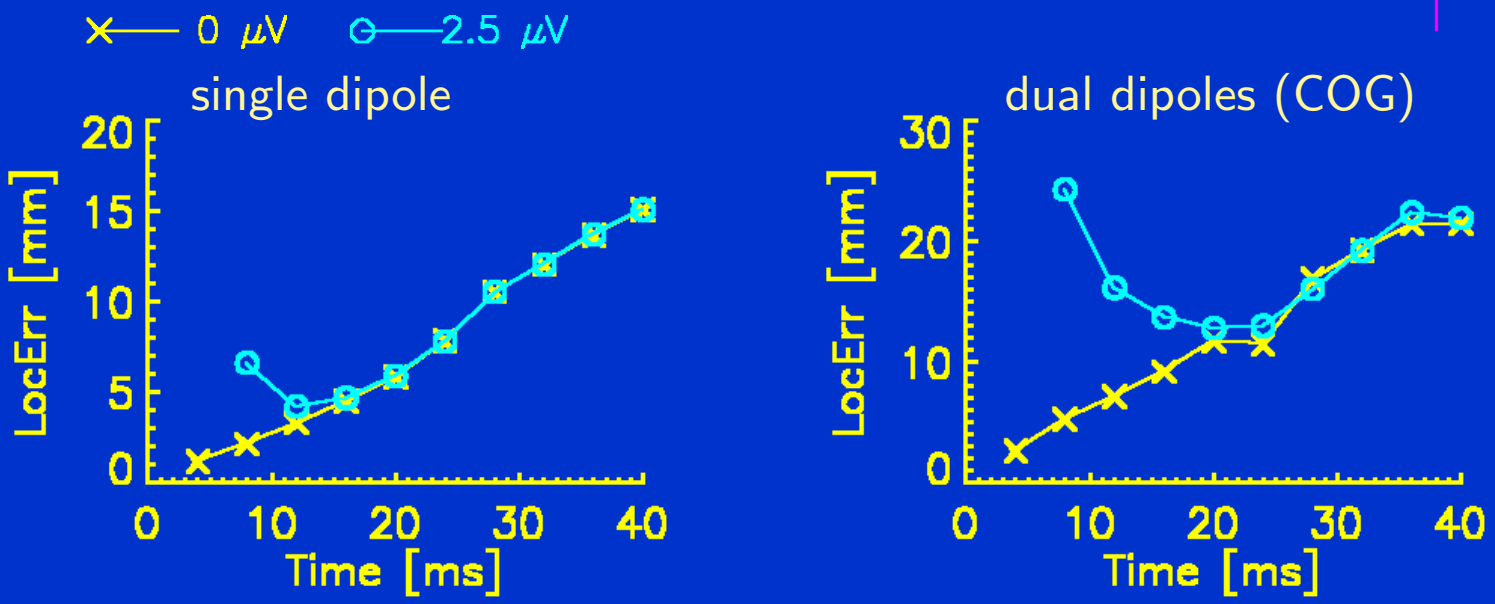

II. Left Lateral single accessory pathway

- projection of activation isochrone surface on the epicardial surface at different time instants (4 to 28 ms after the onset x)
- localization results obtained with a two dipole model (cyan and yellow)
- localization results obtained with a single dipole model (red)

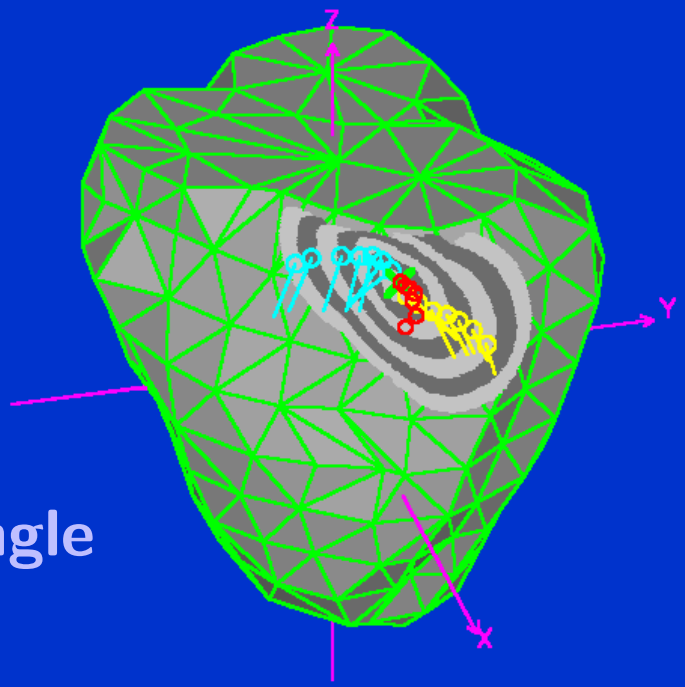

Average localization errors for all 10 single preexicitation sites in presence of noise

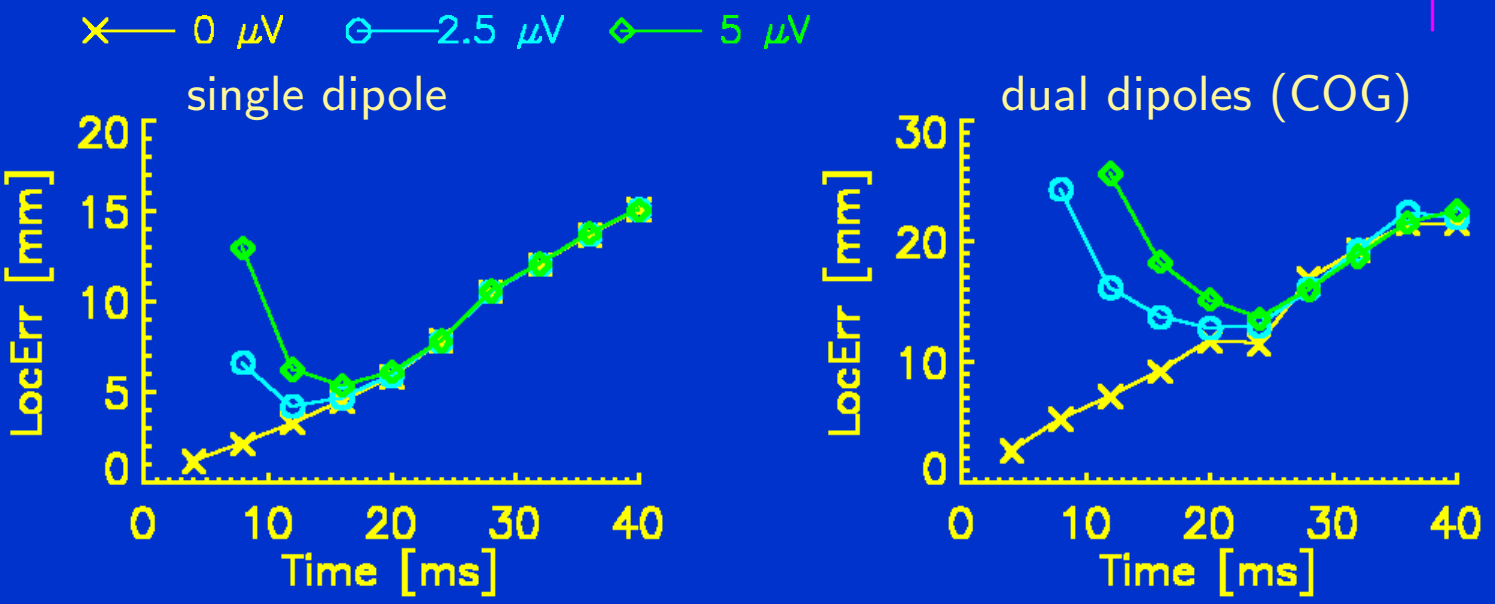

II. Left Lateral single accessory pathway

- projection of activation isochrone surface on the epicardial surface at different time instants (4 to 28 ms after the onset x)
- localization results obtained with a two dipole model (cyan and yellow)
- localization results obtained with a single dipole model (red)

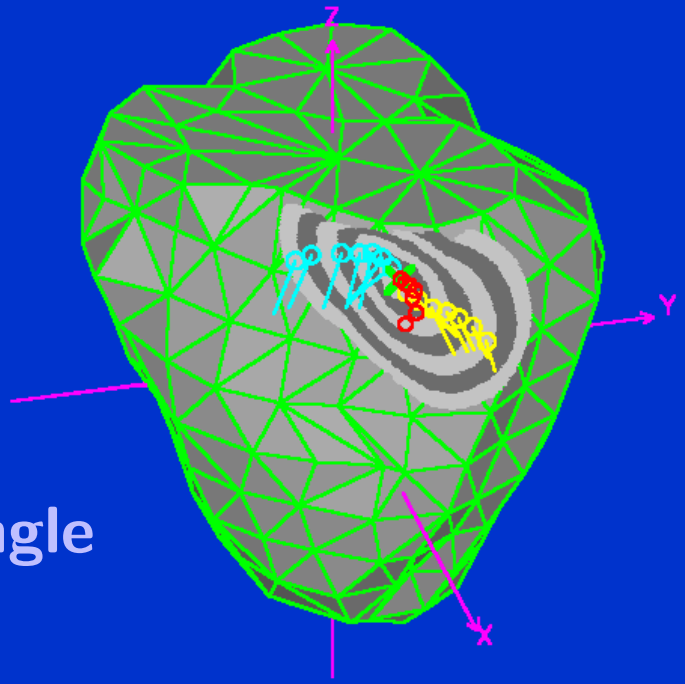

Average localization errors for all 10 single preexicitation sites in presence of noise

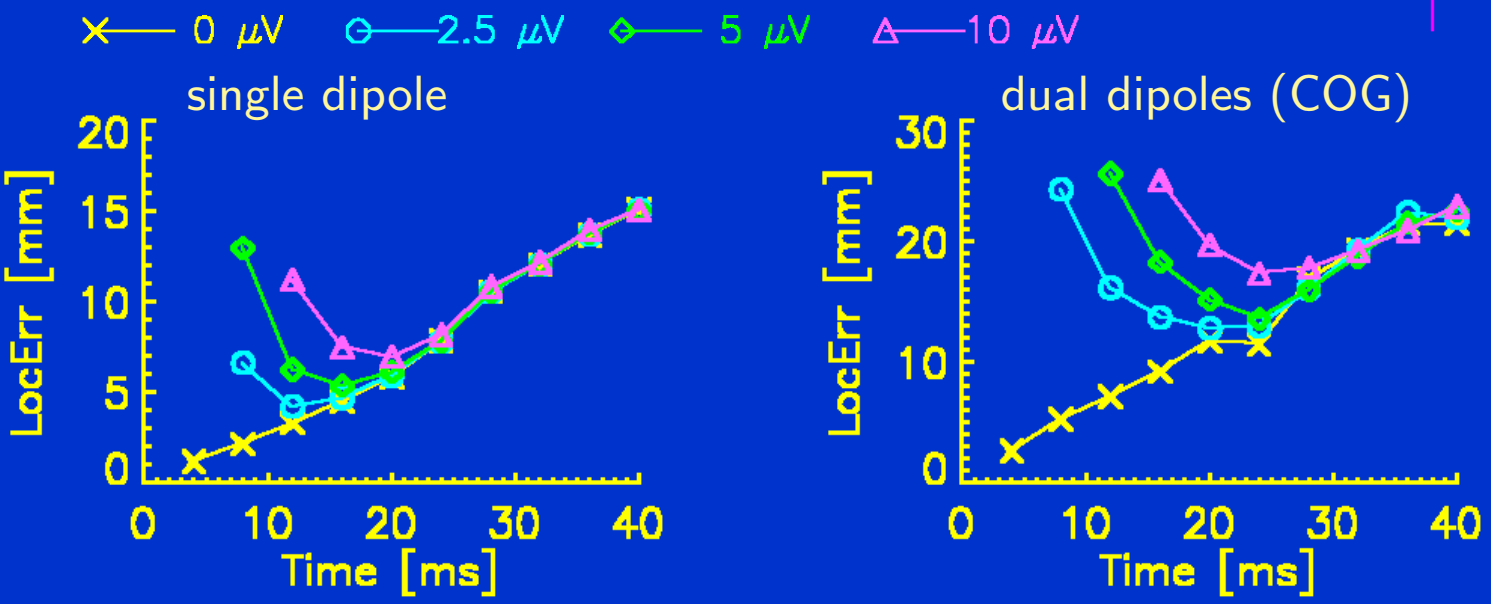

II. Left Lateral single accessory pathway

- projection of activation isochrone surface on the epicardial surface at different time instants (4 to 28 ms after the onset x)
- localization results obtained with a two dipole model (cyan and yellow)
- localization results obtained with a single dipole model (red)

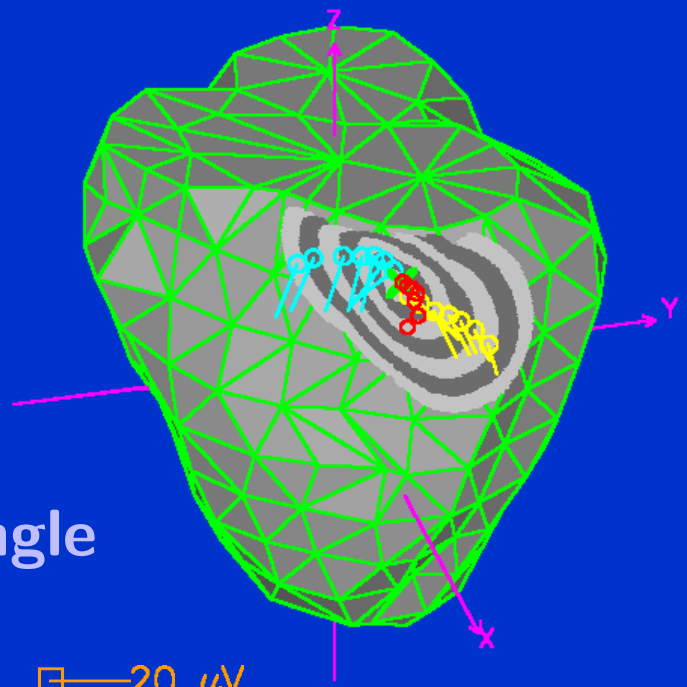

Average localization errors for all 10 single preexicitation sites in presence of noise

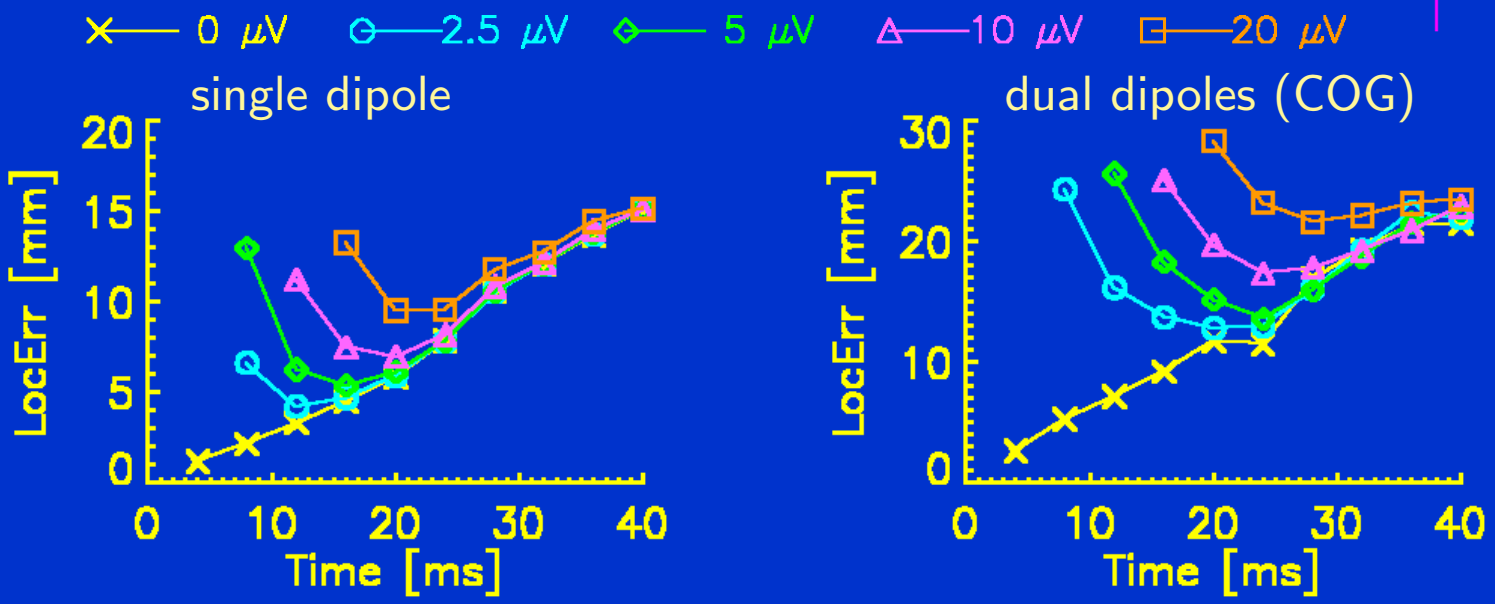

II. Left Lateral single accessory pathway

- projection of activation isochrone surface on the epicardial surface at different time instants (4 to 28 ms after the onset x)
- localization results obtained with a two dipole model (cyan and yellow)
- localization results obtained with a single dipole model (red)

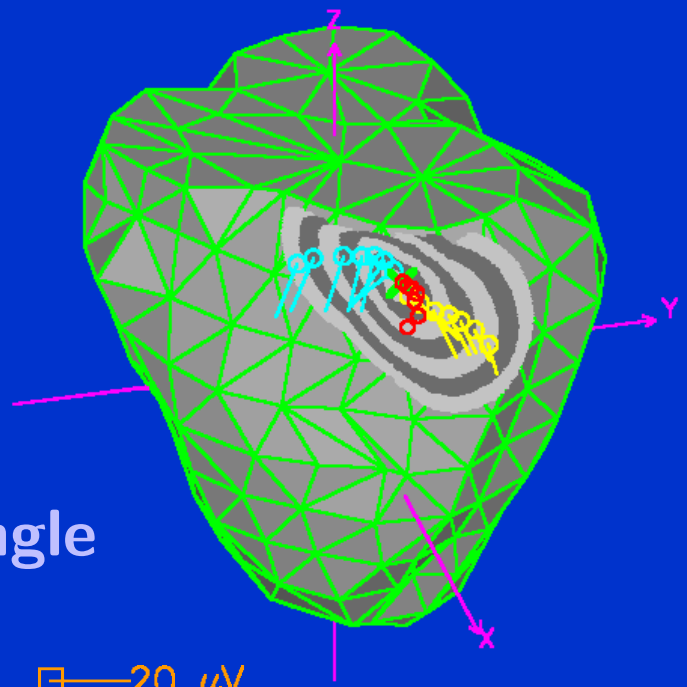

Average localization errors for all 10 single preexicitation sites in presence of noise

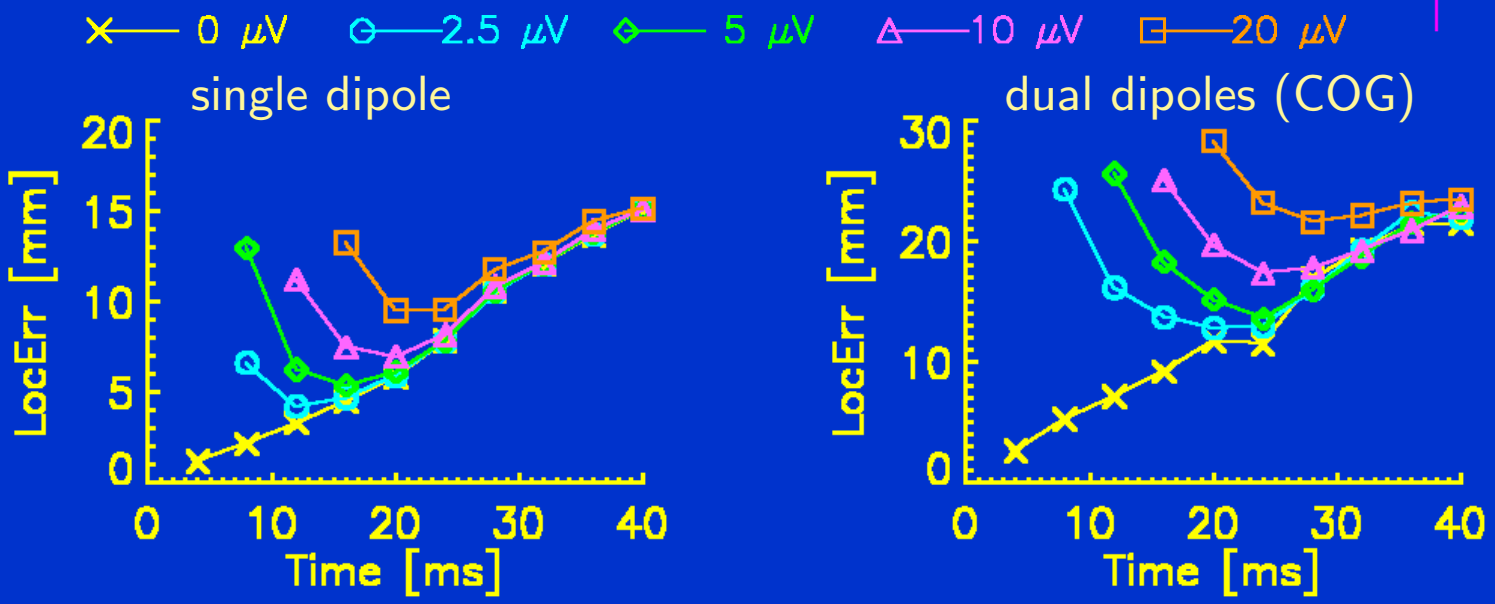

II. Localization of dual preexcitation sites

Right anterolateral / Right lateral dual accessory pathway

Positions of two reconstructed dipoles from 16 to 36 ms after the onset when noise of 5 μV is added to simulated BSPM.

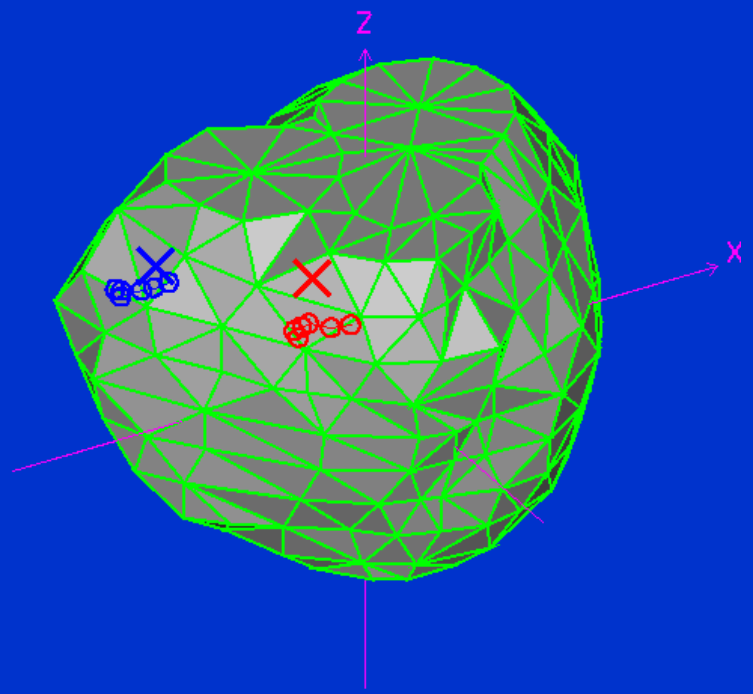

II. Localization of dual preexcitation sites

Right anterolateral / Right lateral dual accessory pathway

Positions of two reconstructed dipoles from 16 to 36 ms after the onset when noise of 5 μV is added to simulated BSPM.

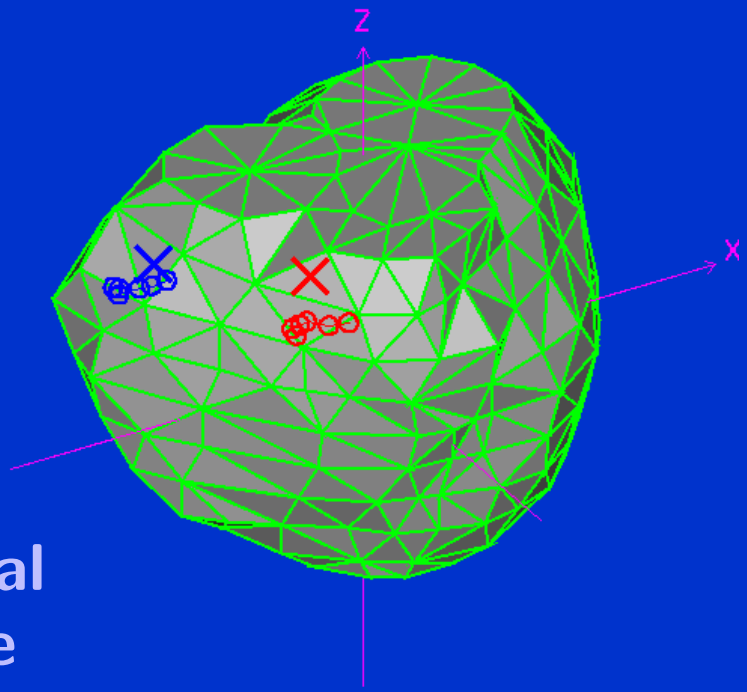

Average localization errors for all 8 dual preexcitation sites in presence of noise

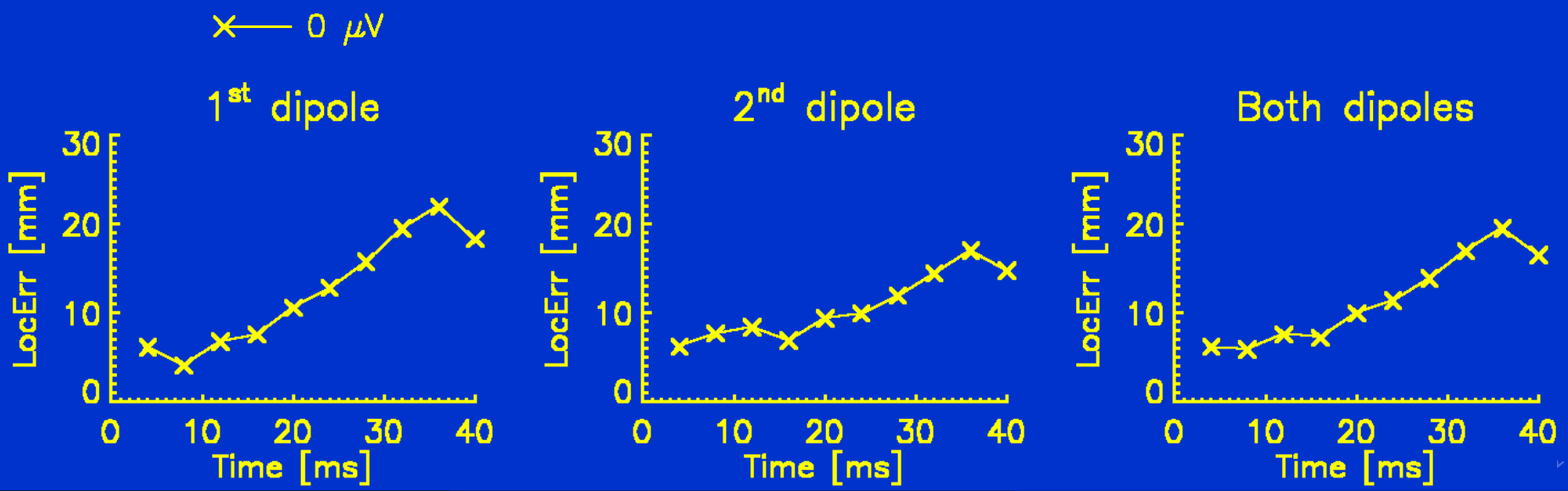

II. Localization of dual preexcitation sites

Right anterolateral / Right lateral dual accessory pathway

Positions of two reconstructed dipoles from 16 to 36 ms after the onset when noise of 5 μV is added to simulated BSPM.

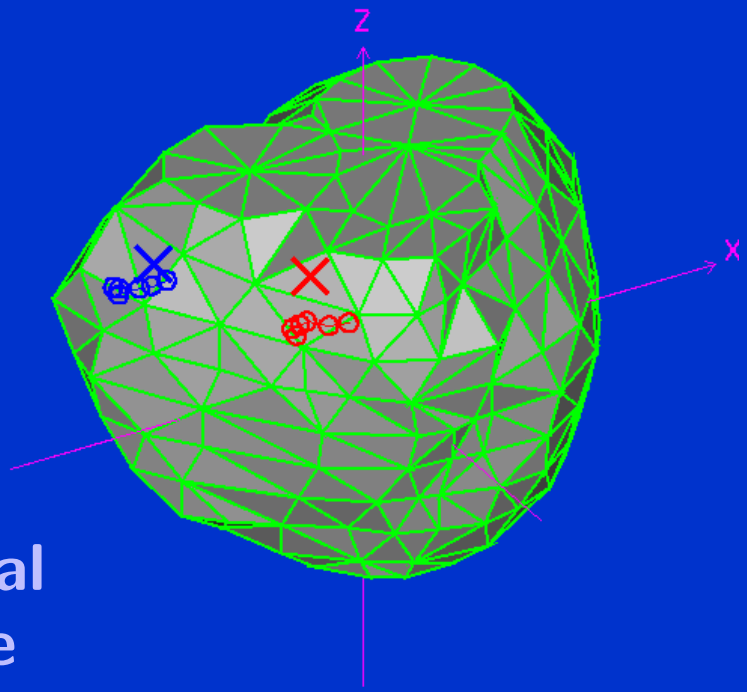

Average localization errors for all 8 dual preexcitation sites in presence of noise

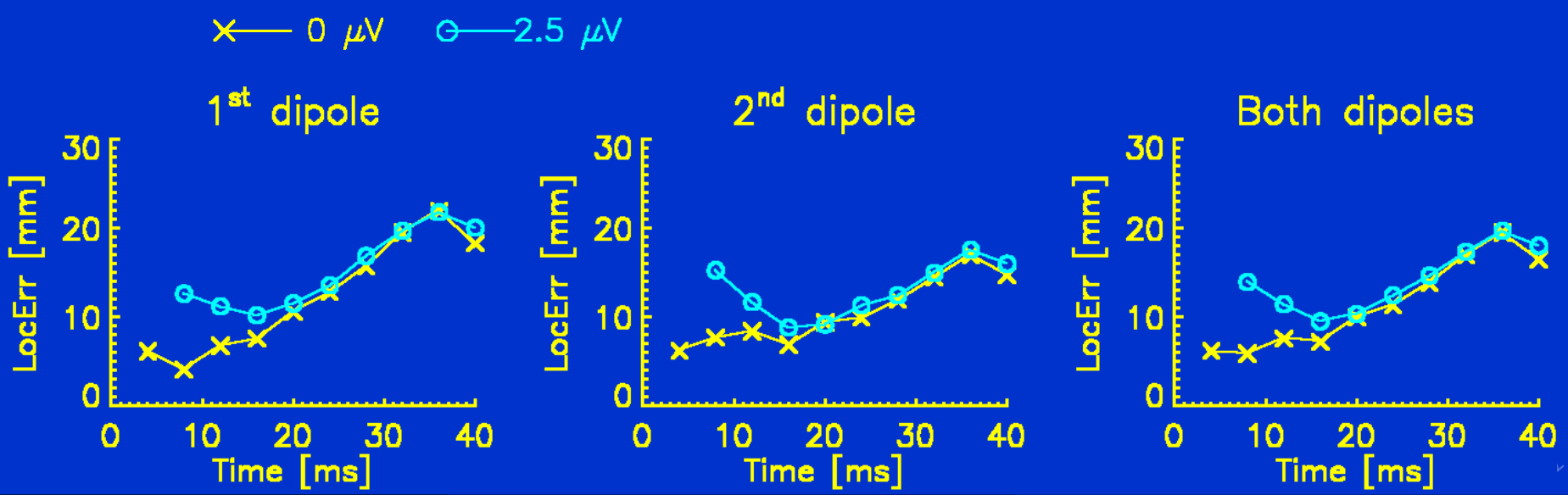

II. Localization of dual preexcitation sites

Right anterolateral / Right lateral dual accessory pathway

Positions of two reconstructed dipoles from 16 to 36 ms after the onset when noise of 5 μV is added to simulated BSPM.

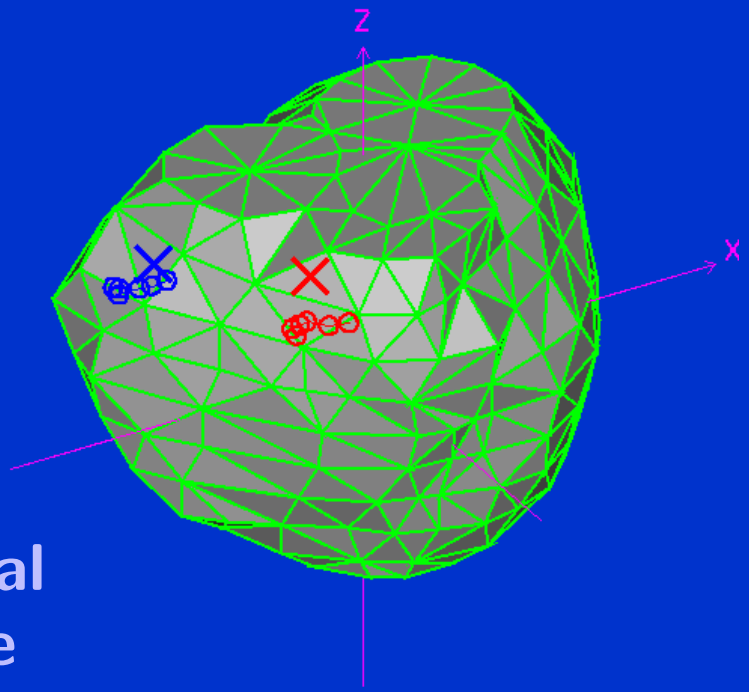

Average localization errors for all 8 dual preexcitation sites in presence of noise

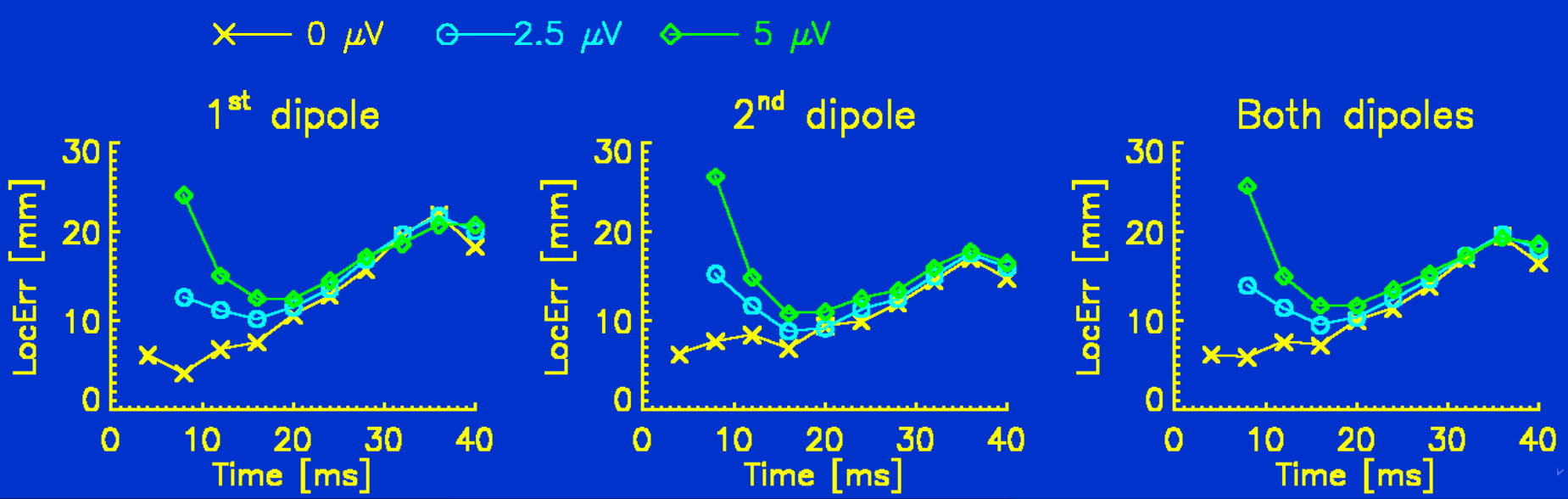

II. Localization of dual preexcitation sites

Right anterolateral / Right lateral dual accessory pathway

Positions of two reconstructed dipoles from 16 to 36 ms after the onset when noise of 5 μV is added to simulated BSPM.

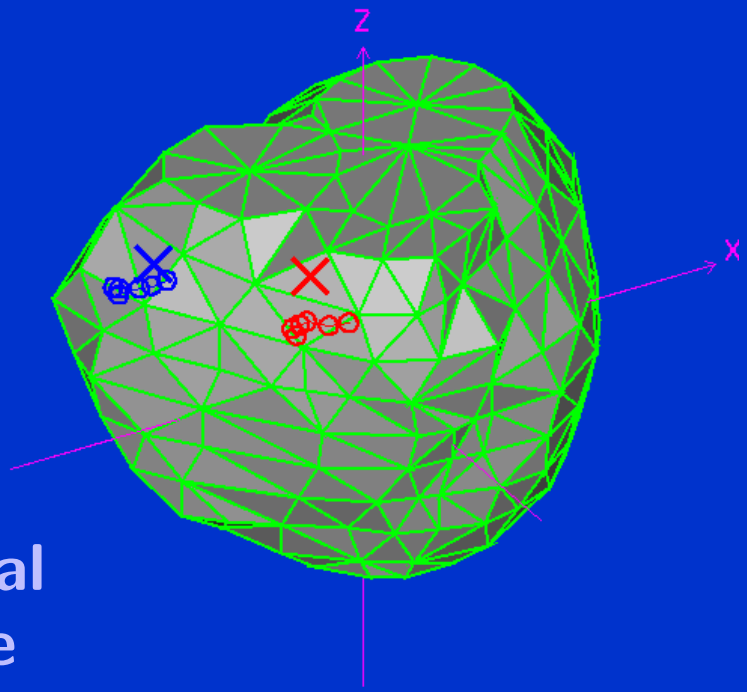

Average localization errors for all 8 dual preexcitation sites in presence of noise

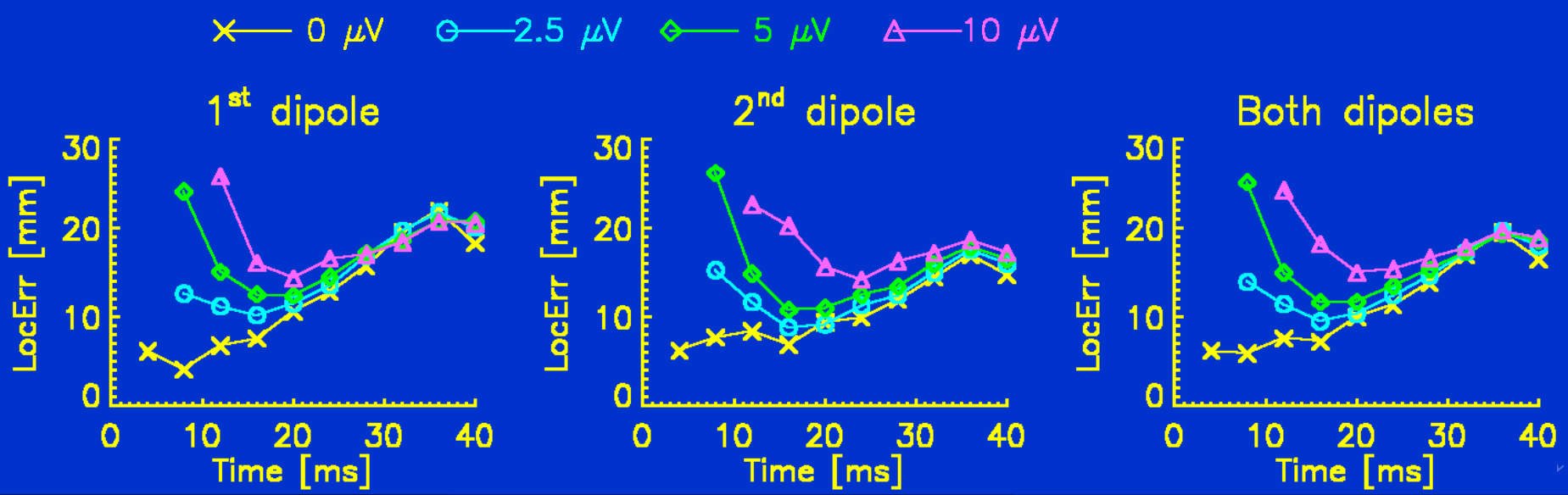

II. Localization of dual preexcitation sites

Right anterolateral / Right lateral dual accessory pathway

Positions of two reconstructed dipoles from 16 to 36 ms after the onset when noise of 5 μV is added to simulated BSPM.

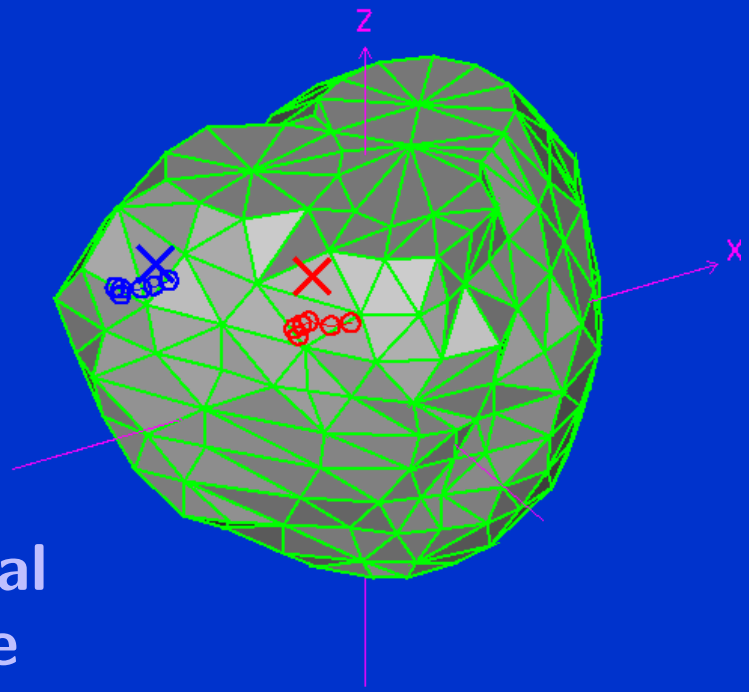

Average localization errors for all 8 dual preexcitation sites in presence of noise

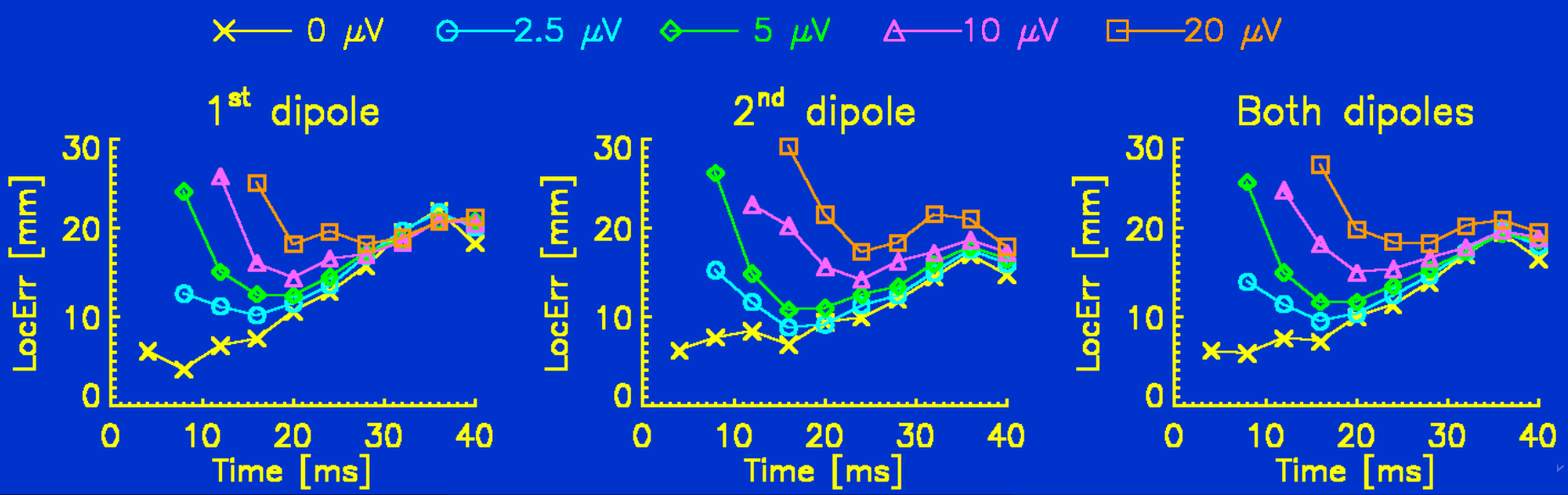

II. Summary of dual accessory pathways localization results

Noise	Range	Average error ± SD First / Second dipole	Optimal time
5 μV	5 to 21 mm	12 ± 6 / 11 ± 6 mm	20 ms
20 μV	8 to 22 mm	18 ± 8 / 18 ± 9 mm	28 ms
Modeling errors: innaccuracies in rendering torzo boundaries			
5 μV	11 to 39 mm	24 ± 18 / 30 ± 13 mm	20 ms

- For a typical noise level of (5 μV) localization errors are in the range of 5 to 21 mm, with the average error ± standard deviation of 12 ± 6 for the first and 11 ± 6 mm for the second dipole, respectively.
- If the noise level is increased by a factor of 4, the average localization errors increase by approximately 50%
- In the presence of modeling errors, where we generated simulated data with the individualized male torso model and we solved the inverse problem with the two-dipole model in the standard torso, the localization errors substantially degraded.

I. Conclusions – simplified conducting sphere model

- In this simulation study, we revisited a well-known bio-electromagnetic model that substitutes true cardiac sources with idealized equivalent single and dual dipole sources.
- We constructed a simplified analytically solvable source and volume conductor model for evaluation electrocardiographic inverse problem solutions.
- Both fitted single current dipoles and dual current dipoles virtually coincided with the original source for high S/N ratios.
- In the presence of higher noise we found that
  - lead systems positioned closer to sources are more efficient and
  - dual current dipole location recovery is sensitive to the distance between the original dipoles.

II. Conclusions – anatomical model of the human ventricles

- Our anatomical model of the human ventricles provided us with means to investigate quantitatively the performance of such a model for more realistic electrocardiographic inverse solutions.
- The results of this study demonstrate that a source model consisting of two dipoles embedded in the realistically shaped torso volume conductor model could be useful in localizing dual accessory pathways providing that
  - we know the torso geometry of a given patient
  - we have a priori knowledge of the presence of dual accessory pathways.
- Both above aspects need to be determined non-invasively to be of clinical use.